Wind and Structures, *Vol. 31, No. 3 (2020) 229-240*
DOI: https://doi.org/10.12989/was.2020.31.3.229

Investigation of crossflow features of a slender delta wing

Mehmet O. Tasci[1], Ilyas Karasu[2], Besir Sahin*[1] and Huseyin Akilli[1]

[1]Department of Mechanical Engineering, Çukurova University, Adana, Turkey
[2]Department of Aerospace Engineering, Adana Alparslan Türkeş Science and Technology University, Adana, Turkey

(*Received May 31, 2019, Revised April 20, 2020, Accepted August 11, 2020*)

Abstract. In the present work, the main features of primary vortices and the vorticity concentrations downstream of vortex bursting in crossflow plane of a delta wing with a sweep angle of Λ=70° were investigated under the variation of the sideslip angles, β. For the pre-review of flow structures, dye visualization was conducted. In connection with a qualitative observation, a quantitative flow analysis was performed by employing Particle Image Velocimetry (PIV). The sideslip angles, β were varied with four different angles, such as 0°, 4°, 12°, and 20° while angles of attack, α were altered between 25° and 35°. This study mainly focused on the instantaneous flow features sequentially located at different crossflow planes such as x/C=0.6, 0.8 and 1.0. As a summary, time-averaged and instantaneous non-uniformity of turbulent flow structures are altered considerably resulting in non-homogeneous delta wing surface loading as a function of the sideslip angle. The vortex bursting location on the windward side of the delta wing advances towards the leading-edge point of the delta wing. The trajectory of the primary vortex on the leeward side slides towards sideways along the span of the delta wing. Besides, the uniformity of the lift coefficient, C_L over the delta wing plane was severely affected due to unbalanced distribution of buffet loading over the same plane caused by the variation of the sideslip angle, β. Consequently, dissimilarities of the leading-edge vortices result in deterioration of the mean value of the lift coefficient, C_L.

Keywords: aerodynamic coefficients; angle of attack; dye visualization; particle image velocimetry; sideslip angle; slender delta wing; vortex bursting

1. Introduction

Aircraft maneuverability is one of the most important features of flight mechanics. The influence of the vortical flows on the aerodynamic characteristics and the behavior of the leading-edge vortices are key areas to investigate the performance of the delta wings as seen from the previous studies such as Payne and Nelson (1986), Escudier (1988), Delery (1994), Lucca-Negro and O'Doherty (2001), Lu and Zhu (2004). The formation and instabilities of vortical flow structures and characteristics of the leading-edge vortices predominantly depend on the design and operation factors that are the sweep angle, Λ, the angle of attack, α, the rolling angle, θ, the sideslip angle, β, the wing thickness, t, the Reynolds number Re, the wing geometries and upstream and downstream flow structures of the delta wing as stated by Nelson and Pelletier (2003). In summary, the configuration of a delta wing and its position in the Freestream flow is very influential on the leading-edge vortices along with their bursting incidence. One of the most fundamental flow events is the leading-edge vortex bursting. The past studies revealing the complexity and features of the development of vortex bursting of the leading-edge vortices were also reported in detail by Hall (1972), Erickson *et al*. (1989), Ericsson, L.E. (1992), Menke *et al*. (1996). The vortex bursting of the leading-edge vortices strongly influences the interaction between surfaces of the solid structure and vortical flows. As stated in the studies of Williamson and Govardhan (2004), Ye and Dong (2014), Sun and Ye (2016) and Ke *et al*. (2019), the effect of the vorticity concentrations and vortex shedding on interactions between the solid surfaces and fluids are significantly high.

The sideslip angle, β has a critical impact on the structures and onsets of the vortex bursting. As a result, it appears to have a significant effect on the aerodynamic features of the delta wings (Johnson *et al*. 1980). It is also seen from the literature that the sideslip angle, β is one of the critical parameters that should be examined and emphasized further. In this respect, Verhagen (2003) pointed out that the sideslip angle, β has more adverse effects on normal forces and pitching moments. Also, the sideslip angle triggers the oscillation of the leading-edge vortex bursting with higher amplitude. Shields and Mohseni (2012) examined the impact of β, the aspect ratio, the planform of the delta wing, the low Re, and the winglet position on the aerodynamic features. They finalized that at a higher α, the main vortices and the tip vortices were combined. This combination was led to complex flow structures that allow increasing the stall angle, α_s delaying the separation and bringing the lift coefficient, C_L to an extreme value. It is shown that the sideslip angle, β causes a decrease in C_L, an increase in friction coefficient, C_f and finally a reduction in rolling moment coefficient, C_m. As a result, Shields and Mohseni (2012) concluded that β is more effective on C_m than C_L and C_D. Karasu (2015) reported that sideslip angles, β varying within the range of $0° \leq \beta \leq 20°$

*Corresponding author, Ph.D. Professor
E-mail: bsahin@cu.edu.tr

http://www.techno-press.com/journals/was&subpage=7
ISSN: 1226-6116 (Print), 1598-6225 (Online)

influences on the vortical flow structure of a delta wing with Λ=70° in side-view plane substantially. When the sideslip angles are varied between β=0° and β=20°, Kelvin-Helmholtz (K- H) vortices were seen clearly. Chen *et al*. (2015) reported that the symmetrical aerodynamic structure of the configurations of the coupled canard wing is distorted under β.

Canpolat *et al*. (2009) explored the flow structures over a non-slender delta wing surface with Λ=40° varying α from 7° to 17°. When the sideslip angle, β was operated, they concluded that the symmetrical time-averaged flow structure was lost; the vortex bursting occurred earlier on the windward side of the delta wing compared to the leeward side. They have also discovered that the main vortices are located on the inboard of the delta wing close to the center or chord axis. Yayla *et al*. (2010) experimentally conducted a study on a 40-degree-swept non-slender diamond delta wing. They examined the impact of the sideslip angle, β on the phenomena of vortex bursting by means of dye observation under α=7° and α=10° in the plan-view plane. They finalized that there were no well-defined alterations in the site of vortex bursting up to β=4°, but in the increment more than β=4°, this vortex bursting location advances towards to the apex of the delta wing on the windward side. Conversely, asymmetric vortex bursting on the leeward side appears to slide into the inner region of the delta wing. Canpolat *et al*. (2012) studied the impact of β on the flow behavior of a 40-degree-swept delta wing in the crossflow plane. The experimental representations indicate that when the delta wing has a higher β, the center of foci, F_1 and F_2 move downward away from the delta wing surface at the same crossflow plane. Investigation of the effects of *Re* downstream of the vortex bursting for non-slender delta wing having Λ=35° is conducted by Zharfa *et al*. (2016). They concluded that the influence of *Re* ranging from 10^4 to 10^5 on flow behaviors is weak.

The studies from the literature that commonly expose the impact of the sideslip angle, β on the aerodynamics of the non-slender delta wings. The aim of the current study targets to provide a comprehensive information about the physics of flow on the slender delta wing with the sweep angle of Λ=70° in the crossflow plane. Gursul *et al*. (2005) stated that aerodynamics of non-slender delta wings differ significantly comparing to the flow structures developed over more slender planforms (Λ≤65°) as a function of α and *Re*. Particularly, considering the variations of sideslip angle, β there is not enough research work providing information about the aerodynamics of slender delta wing with Λ=70° in the crossflow plane under the variations of β using particle image velocimetry (PIV), so that one can visualize the flow domain quantitatively.

In this study, it is aimed to observe how the flow structure formed during the maneuver of the delta wing is affected under variations of α and β. The ability of the delta wing is impaired under the variation of α and β. The point that distinguishes this study from previous studies is to analyze the variation of the aerodynamic features on the slender delta wing with Λ=70° visualizing sets of instantaneous crossflow images to reveal physics of flow in detail. The impact of the sideslip angle, β on the vortical flow structures of the delta wing in the crossflow plane was not quantitatively examined using the PIV technique to display the unsteady flow physics. The main features of a pair of primary vortices revolving in opposite directions, the vorticity concentrations downstream of vortex bursting in crossflow planes of a delta wing can only be identified by quantitative observation of instantaneous flow data employing the PIV method. In previous studies, the experiments such as visual observations, pressure measurements, pointwise velocity measurements and force measurements have only been conducted. To reveal the physics of the vortical flow structures, we need to examine the instantaneous turbulent statistics based on the distribution of instantaneous velocity vectors in crossflow fields obtained by the PIV method in the water channel. In addition, aerodynamic coefficients, C_L and C_D using force measurements in the wind tunnel were evaluated.

2. Experimental arrangements

The water channel was 1000 mm wide, 750 mm high and 8000 mm long, which was constructed from transparent Plexiglas with a thickness of 15 mm. Water channel had two fiberglass tanks at the entrance and exit of the channel and water was delivered from downstream tank to upstream tank. Just before reaching the test section, fluid first was transported into a calming reservoir and then, conveyed through a flow straightener unit before passing through 2:1 duct contraction. Arrangements such as tanks, chamber, and honeycomb are located to ensure turbulence intensity lower than 0.4%. Also, a 15kW electric driven pump which has a frequency control unit to set the flow speed was used. The chord length, *C* and the thickness, *t* of the delta wing with a sweep angle of Λ=70° was taken as 180 mm and 5 mm, respectively. The ratio of the thickness to chord length was t/c=0.0278. Also, the bevel angle at the leading edge of the delta wing was 45°. The Reynolds number determined according to the length of the chord; *C* was kept constant as $Re=2\times10^4$ throughout the experiments. In PIV experiments, 1000 instantaneous images were analyzed to obtain the time-averaged results precisely. Before recording quantitative flow data with the PIV system, it was decided to examine the flow structures using the dye visualization technique to see how the flow structures behave in a water channel under the variations of α, and β. At the beginning of the experiments, it was also decided to have a brief and rough impression concerning the flow properties of the delta wing. For this purpose, the dye image creation method was initially employed. In general, the water-dye mixture having tiny amounts of Rhodamine 6G powders were injected into the flowing water and the dye starts shining with different tones of green color underexpose of laser light and the dye provides visual evidence relating to the structures of flow over a measurement plane. The dye mixture was kept in a small bowl placed above the channel. The dye was passed through a narrow gap situated lengthwise with the delta wing axis towards its apex and injected by a thin plastic pipe. The mirror was positioned at a location which was 900 mm (x/C=5) far from the trailing

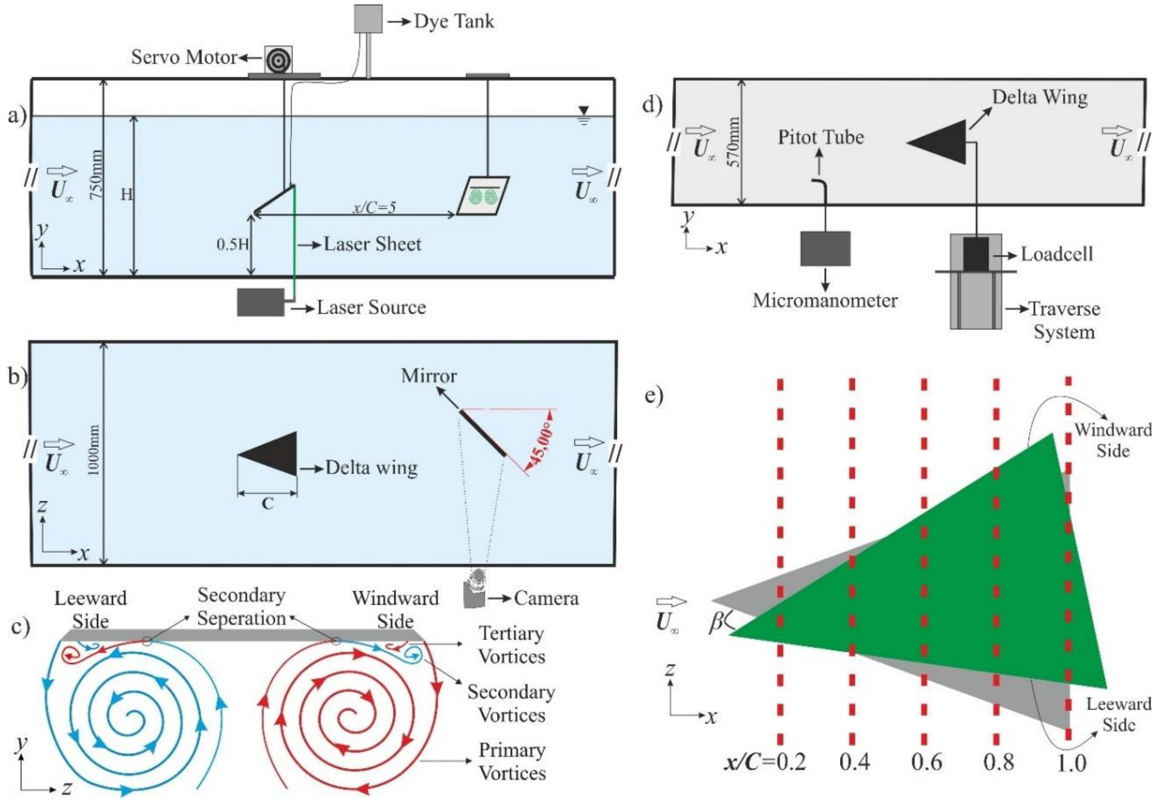

Fig. 1 The schematic representation of a) the experimental setup of a the water channel in side-view plane and b) in plan-view plane, c) the vortical flow structure of a delta wing in the crossflow-view, d) the experimental setup of a wind tunnel in side-view plane, and e) the change of measuring locations, *x/C* and sideslip angle*, β*

edge of the delta wing to avoid affecting the flow behavior. The mirror was turned 45° from the free-stream flow direction taken as a reference line to ensure that the crossflow plane of the measuring section is accurately displayed on the camera. Sony HD-SR1 video camera having 24 fps (frame per second) was used to capture the images of flow field over crossflow plane across the delta wing from dye visualization videos. Images were taken by special pose grabber software of Sony. The same experimental setup was used for a quantitative flow observation using the PIV system. The PIV system is the velocity measuring device to take the time-dependent velocity distributions over a flow field. Neutrally buoyant silver-coated spherical glass particles with 10 µm-diameters were lightened by a double-pulsed laser beam at a given period to generate views documented on a CCD camera.

This image capture received 15 frames per second with a resolution of 1600×1200 pixels. The particle density in the interrogation area was about 35. Bad vectors were eliminated using CLEANVEC software which was written by Meinhart and Soloff (1999). A cross-correlation technique, with 32×32 pixels interrogation windows, was selected to be used with an overlap of 50% to assess the velocity field. During the experiment, a laser beam was set normal to the flow direction. Uncertainty of the velocity measurements was lower than 2% as stated by Ozturk *et al.* (2008). As shown in Fig. 1, the servo motor was operated to control α and β, precisely. All experiments were conducted on the suction side (underside) of the delta wing to reveal the behavior of the flow structure and the location of the vortex bursting of the delta wing. The representation of the experimental setups in water channel and wind tunnel, the general knowledge of the vortical flow structure of a delta wing in crossflow plane and the change of measuring locations, *x/C* and sideslip angle, β, were shown in Fig. 1. The test zone of the wind tunnel where the delta wing and measuring elements are positioned has a square cross-section with dimensions of 570 mm × 570 mm and a length of 1000 mm. The Pitot tube was used to control the desired speed. F_L and F_D were measured using the formulas of $C_D=F_D/\rho U^2A$ and $C_L=F_L/\rho U^2A$ to determine the lift and drag coefficients, C_L and C_D where ρ (kg/m^3) is the density of water, U (m/s) is the free-stream velocity, A (m^2) is the projection area with the help of F_L and F_D values.

3. Result and discussion

In the present study, the focuses are given on the essential features of the leading-edge vortex bursting, its occurrence and the physics of vorticity observed qualitatively and quantitatively using two kinds of experimental techniques over the crossflow plane of the delta wing. For these experimental studies, the angle of attack is changed from α=25° to 35° and the sideslip angles are varied as β=0°, 4°, 12°, and 20°.

For quantitative observations, the experiments were

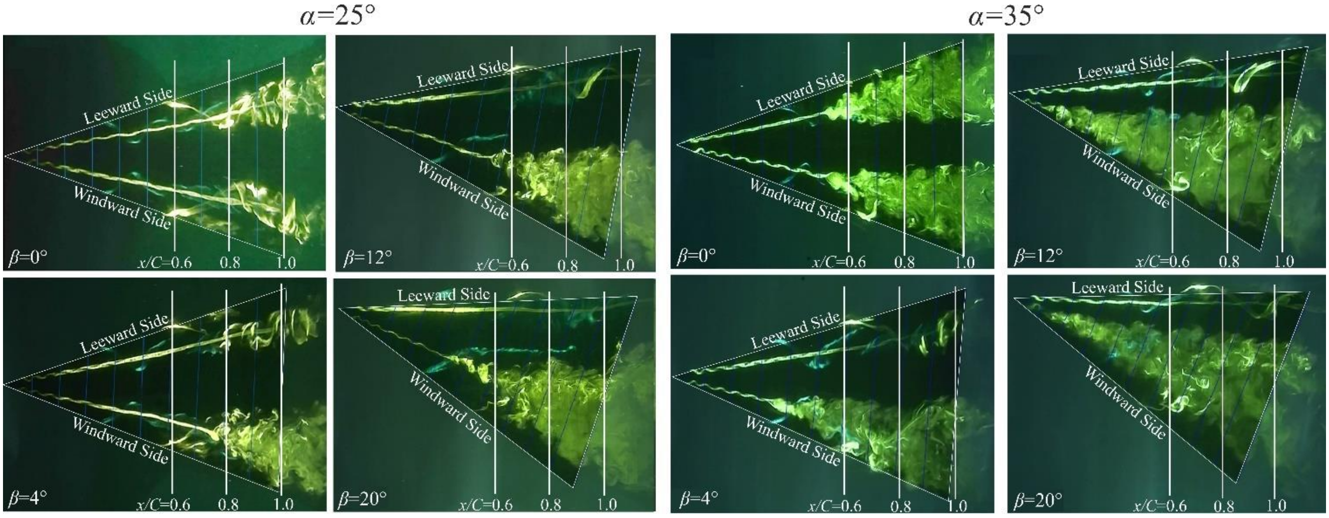

Fig. 2 Presentation of leading-edge vortices along the surface of the delta wing for α=25° and 35° under the variation of sideslip angle, β (Karasu *et al*. 2015)

fulfilled using the two-dimensional PIV technique. The root mean square (RMS) of velocity fluctuations, v_{rms} and w_{rms} over a defined flow field, patterns of streamlines, $<\Psi>$ and vorticity contours, $<\omega^*>$ are analyzed to reveal the flow mechanism in crossflow planes close to the surface of delta wing vertically. The dye visualizations in the plan-view plane reported by Karasu *et al*. (2015) provide the view of the vortical flow structures over the surface of the similar delta wing which was used in the present study as seen in Fig. 2. However, in the present study, the visualization of dye observations was conducted in a crossflow plane to show the influence of the sideslip angles, β on the vortical flow structures. This study allows us to correlate between crossflow-view and plan-view planes and to understand better how sideslip angles, β cause changes in the vortical flow structure along the slender delta wing. The interaction between the leading-edge vortices on both sides of the chord axis along the surface of the delta wing was observed as reported by Karasu *et al*. (2015). Similarly, the dye observation in the crossflow plane shows that the intensity of the interactions between the leading-edge vortices situated on both sides of the chord axis varies substantially as a function of β as reported in Fig. 3. The locations, x/C of crossflow planes are indicated by white lines drawn on the plan-view images shown in Fig. 2. The aerodynamic features of a delta wing with β=0° were generally investigated by force measurement in the previous studies. However, in the present study, the PIV technique was used to focus particularly on the aerodynamic features of a delta wing under the variations of the sideslip angle to reveal the physics of flow mechanism which affects homogeneous of buffet loading over the delta wing surface. The x/C planes are located at five different locations along the chord axis for dye observations such as x/C=0.2, 0.4, 0.6, 0.8, 1.0 and three different locations for the instantaneous measurements with the PIV technique at locations such as x/C=0.6, 0.8, and 1.0. However, only a few selected images were included in the study, in other words, the results determined from instantaneous velocity readings under the effects of β=4° and β=8° were not included. The dye visualization results of β=4° were only shown to prove that this sideslip angle, β has a minor effect on the vortical flow structure over the delta wing surface.

3.1. Qualitative observation

The dye visualization technique was used over the crossflow plane to observe vortical flow behaviors after the onset of vortex bursting. The different colors on figures were used to show the path of the leading-edge vortices clearly for both qualitative and quantitative results. As shown in Figs. 2, 3 and 4, the changes in the location of vortex bursting are illustrated based on the variations of the sideslip angle, β. The mirrored locations of vortex bursting in crossflow plane, x/C, are lined up on the projection surface of the delta wing, and hereby, windward and leeward sides of the delta wing are as seen in Figs. 3 and 4.

When the delta wing has β=0°, the time-averaged structures of vortex bursting and its location at both sides ofthe chord axis are quasi-symmetric in the macro scale as demonstrated in Fig. 2. The purpose of this work is to study the vortical flow structures in crossflow plane. However, the optimal evaluation of the vortical flow structures in the plan-view plane in connection with related flow structures in crossflow plane is inevitable. At different α, and β, some features of vortices such as the swirling velocities, the size and the magnitude of the leading-edge vortices and the bursting locations are different under the variation of β (Karasu *et al*. 2015). For example, the leading-edge vortex bursting does not generally occur over the delta wings at α=25° or lower. But, as shown in line 1 column 2 of Fig. 2, when the delta wing is positioned at β=12° and α=25°, the leading-edge vortex bursting occurs on the windward side of the delta wing at x/C=0.6. But the other leading-edge vortex passes along the delta wing without vortex bursting. However, if the angle of attack and sideslip angle are adjusted as α=35°, and β=20°, the leading-edge vortex bursting occurs much earlier on the windward side. The dye visualization indicates that the primary vortex bursting on the windward side having a larger size with a greater

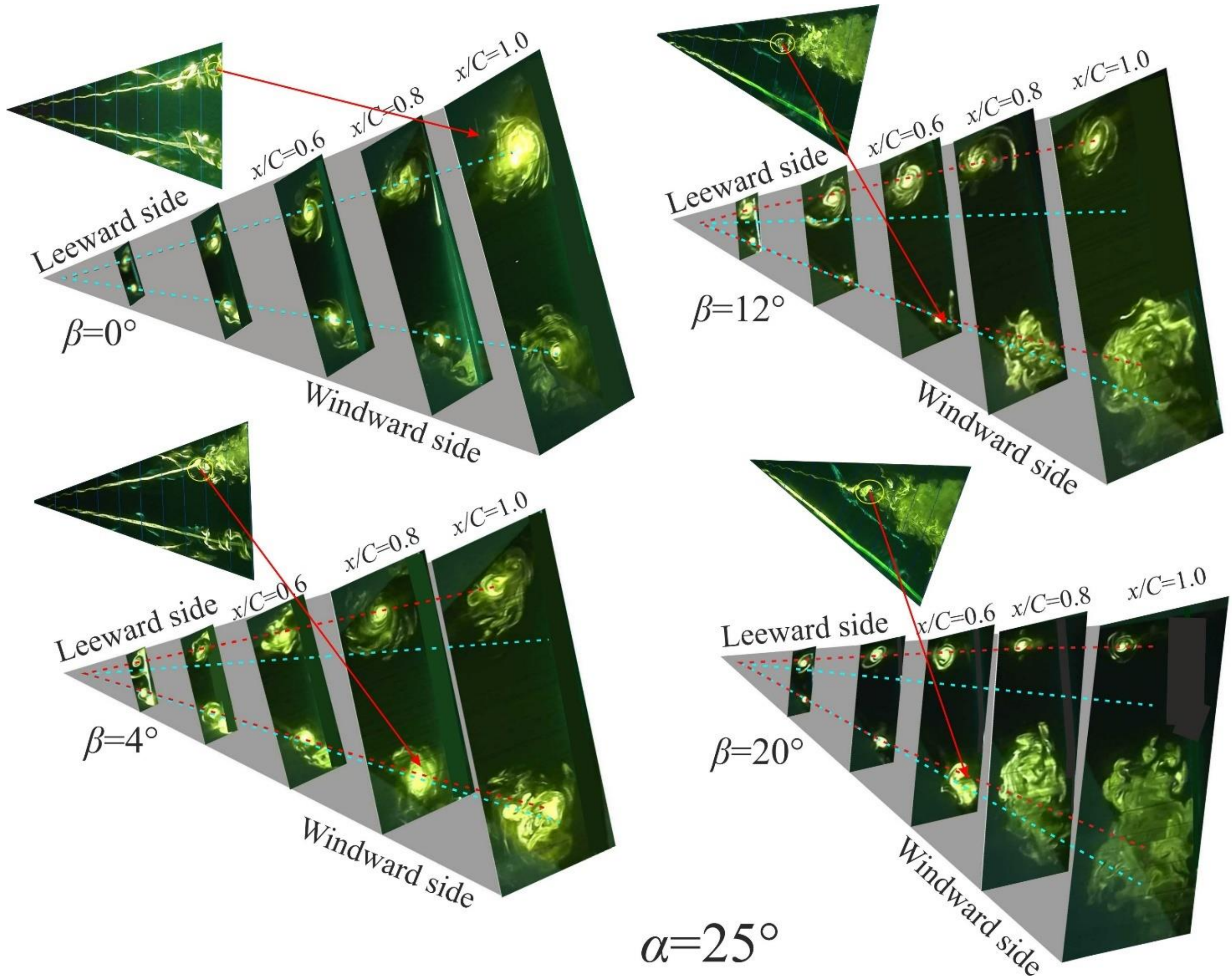

Fig. 3 Presentation of leading-edge vortices over crossflow planes under the variations of the sideslip angle, β. The blue dashed lines present the trajectory of leading-edge vortices for $\beta=0$. The red dashed lines present the trajectory of leading-edge vortices for $\beta>0$.

vorticity magnitude generated after the vortex bursting occurs near the apex of the delta wing, but the other leading-edge vortex moves on the leeward side, towards the trailing edge of the delta wing without breakdown due to an increase of sideslip angle as observed in Figs. 3 and 4 in connection with Fig. 2. The free-stream flow towards the pressure side of the delta wing was not conveyed equally over both sides of the delta wing under the influence of β. Due to this fact that more free-stream fluid is transported on the leeward side of the delta wing resulting in a stronger leading-edge vortex than the case of β=0°. In general, the axial velocity along the central axis of the leading-edge vortex is expected as large as two times higher than the free-stream velocity as stated by Hall (1972), on the other hand, the same axial velocity may go up to five times higher than the free-stream velocity as stated by Gursul and Wang (2018) depending on the delta wing parameters in the case of β=0°. In fact, as the sideslip angle, β increases the central axis velocity of the leading-edge vortex increases even more because there is more fluid flowing towards the leeward side. The gradual expansion of leading-edge vortex core along its central axis causes a gradual increase of the pressure gradient along the leading-edge vortex core axis which progressively becomes more opposing to leading-edge vortex bursting. In summary, the magnitude of velocity in the region of the vortex bursting of the windward side is slower than the leeward side and it means that we can easily see the diameter difference of vortices between two sides which is visualized qualitatively as revealed in Figs. 3 and 4. Thus, the size of the vortical flow structures increases step by step after the bursting of the leading-edge vortices as the wake-like flow moves toward the rear edge of the wing. The focus of this study in terms of the locations of the leading-edge vortices along the delta wing on the windward side is generally after the vortex bursting (wake) area for both angles of attack, α. One of the aims of the present study is to focus on regions where the position the bursting of the leading-edge vortices and the subsequent region on the windward side of the delta wing becomes very sensitive to β under both angels of attack, α.

The large-scale vorticity concentrations enlarge and move towards the center of the delta wing as β increases gradually. The large-scale vorticity concentrations interact with the small-scale vorticity concentrations after β=12°. As

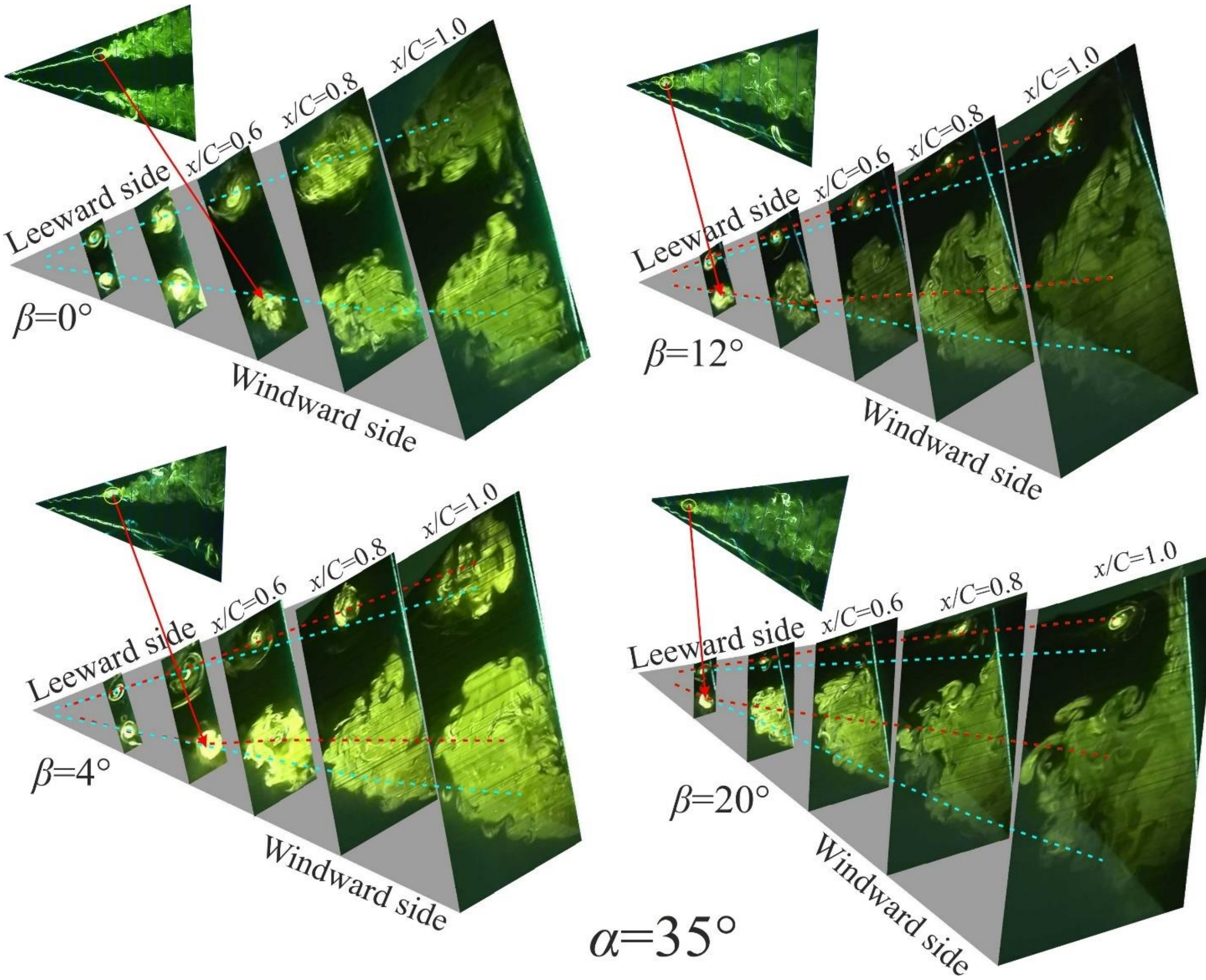

Fig. 4 Presentation of leading-edge vortices over crossflow planes under the variations of the sideslip angle, β. The blue dashed lines present the trajectory of leading-edge vortices for $\beta=0$. The red dashed lines present the trajectory of leading-edge vortices for $\beta>0$.

the small-scale vorticity concentration approaches the delta wing's leeward side, these clusters of vortices shrink in size. The leading-edge vortex on the leeward side continues without bursting as β increases. The outer boundary line of the wake flow domain travels slowly away from the wing surface and the separated flow domain expands in size at the same time while the measuring cross-section normal to the cord axis moves downward in the direction of free-stream as observed from video records of dye visualization.

3.2 Quantitative observation

As evidenced by visual dye experiments, symmetrical flow characteristics occur at macro scale on both sides of the central axis of the delta wing with β=0° as reported about several applications of delta wings by many researchers such as Verhagen (2000), Sahin *et al*. (2001), Ozgoren *et al*. (2002) Yaniktepe and Rockwell (2004 and 2005), Sahin *et al*. (2012), Meng *et al*. (2018) and others. On the other hand, instantaneous flow data do not reveal symmetrical flow characteristics after a point of the primary vortex bursting. Since flow structures are extraordinarily unsteady and have random motions as demonstrated by the dye visualization as well as animations of instantaneous turbulent flow statistics derived from instantaneous velocity readings measured by the PIV system. Figs. 5 and 6 present time-averaged patterns of streamline for α=25° and α=35°, respectively. A well-defined reversed flow clusters called foci are detectable through streamlines. The locations of the foci, F, saddle points, S and bifurcation lines, L^+ are symbolically illustrated in line 1 column 3 in Fig. 5 and in Fig. 6 and they are applicable for all images in both figures. A couple of stagnation points presented as S_1 and S_2 are situated below F_1 and F_2. The midpoints of main vorticity concentrations, F_1 and F_2, slides towards the left-hand (leeward) side of the delta wing while increasing the sideslip angle from β=0° to β=20°. Saddle structures with two stagnation points occur along the borderline of core and wake flow regions. The positive bifurcation lines, L^+ define the border where the core flow region meets with the wake flow region. A similar description is also expressed by Yayla *et al*. (2013), Canpolat *et al*. (2012) Taylor and Gursul (2004) and it is seen that flow fields are incredibly sensitive to the change of α under the effect of β. The

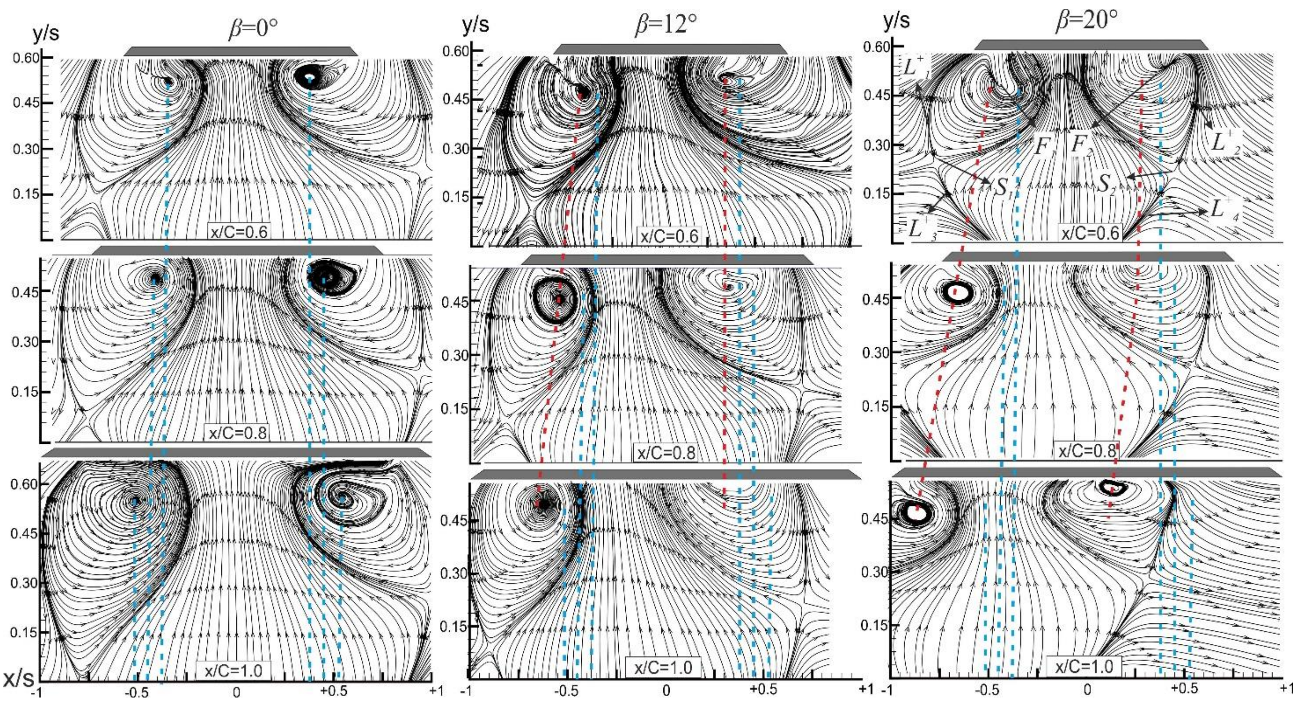

Fig. 5 Patterns of time-averaged streamline, <Ψ> for α=25° with different colorful paths for different sideslip angle s, β. Blue and red lines indicate the change of the locations of foci, F_1 *and* F_2.

topological properties of the vortical flow structure can be distinguished as seen in Figs. 5 and 6, for instance, lines designed by positive L^+_1 and L^+_2 are starting from the side edge of the delta wing proceed through the crossflow plane in the suction side and move towards both S_1 and S_2 on both sides of the delta wing. On the other hand, the lines symbolized by L^+_3 and L^+_4 emerged from the nodal point, *N* which is taken place outside of images and emerge from right and left-hand sides of nodal points, *N* extend towards S_1 and S_2 developing a closed enclose with a parabolic profile as indicated in Figs. 5 and 6.

The mid locations of reversing and concentrated streamlines that present focal points slide significantly to the left-hand (leeward) side of the delta wing, as seen in Fig. 6, due to upgrading from β=0° to 20° at α=35°. The displacement of F_1 and F_2, as well as S_1 and S_2, to the left and the cross-sectional area of the windward side vortex, considerably increases with the growth of *x/C*. The topology of streamlines, <Ψ> showing a well-defined rotational flow structure indicates that the flow structure is asymmetric under the effect of β. By the contour of streamlines, <Ψ> well-defined focal points and saddle points are displayed along the borderline where the core flow region meets with the wake flow region. These intermediate bifurcation lines, L^+_1, L^+_2, L^+_3, and L^+_4 specify the boundary between the free-stream flow region and the wake flow region.

Although the velocity of the vortex core is higher than free-stream velocity before the vortex bursting, the velocity of the vortex core is slower than free-stream velocity after the vortex bursting as stated by Gursul and Wang (2018). The more the circulation increase, the more the diameter of the leading-edge vortices increase. The swirling velocity increases with an increase of circulation. However, the pressure gradient throughout the leading-edge vortices becomes more contrary compared to the circulation as specified by Hall (1972). Besides, the pressure gradient decreases with the increase of β. The interaction between the leading-edge vortex on the windward side and the surface of the delta wing increases when β increases. The focal point of the windward side of the delta wing, F_2 shifts upward depending on the increase of β. It is seen in line 3 columns 2-3 in Fig. 6 that the streamlines, <Ψ> of the windward side of the delta wing become a chaotic cluster and move toward to the center of the delta wing. Besides, it is seen that the central point on the windward side of the delta wing begins to disappear and the instability of the vortical flow starts increasing when α=35° and β=12.

In summary, the sideslip angles, β and the angles of attack, α alter the vortical flow structures significantly. Taking the chord axis as a reference line on the left-hand side or leeward side, swirl patterns of streamline keeps its structures without deforming under all β, as seen in columns 2-3 in Fig. 6. A serious asymmetric structure is formed the delta wing and the stall occurs on the windward side of the delta wing due to this asymmetric structure. Stalled flow dominates most of the delta wing surface. The distance between the delta wing surface and both locations of S_1 and S_2 increases as seen in line 3 in Fig. 6.

Root mean square (RMS) of transverse, v_{rms} and vertical, w_{rms} velocity components at the angles of attack of α=25° and α=35° for *x/C*=0.8 and β=20° were presented in Fig. 7, respectively. The downstream region of the leading-edge vortex, the observation of cinema (animation) of instantaneous images of the flow domain demonstrates that the magnitude of the velocity fluctuations is significantly high and covers the whole domain of swirling flow. This fluctuating flow domain expands up to the delta wing

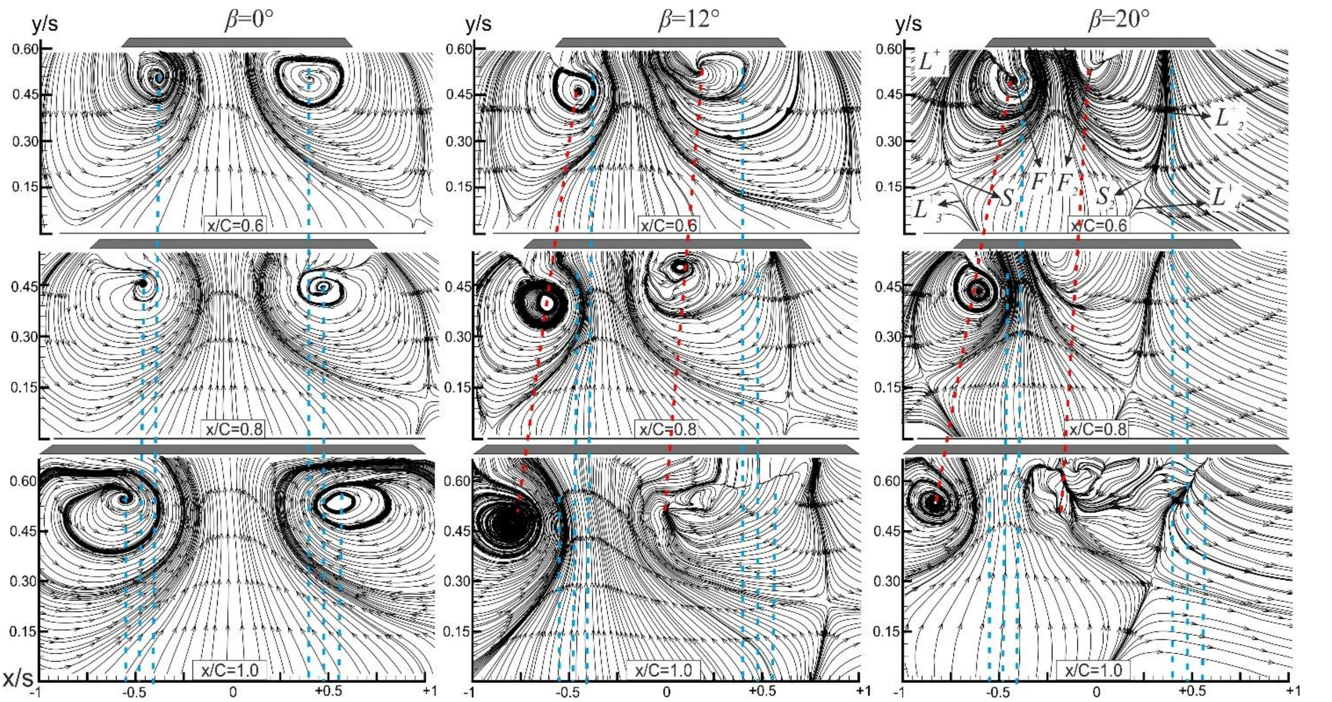

Fig. 6 Patterns of time-averaged streamline, $<\Psi>$ for α=35° with different colorful paths for different sideslip angles, β. Blue and red lines indicate the change of the locations of foci, F_1 *and* F_2.

surface causing a highly unstable buffet loading under α=25° and β=20° at *x/C*=0.8. As seen from Fig. 7, the zone of maximum values of v_{rms} and w_{rms} moves away from the delta wing surface towards the central points of the swirling flow domain where the magnitudes of the highest time-averaged RMS velocity components measured at α=35°. There are two well-defined swirling flows which intensely influence each other as seen in line 2 in Fig. 7. Swirling flow 1, *Sf1* which takes place on the windward side expands large enough to interact significantly with Swirling flow 2, *Sf2* which occurs on the leeward side. Besides, the high magnitude of velocity vectors, $<V/U>$ clearly appears along the periphery of *Sf2* as seen in the third line of Fig. 7.

Time-averaged dimensionless vorticity $<\omega^*>$ patterns are presented in Figs. 8 and 9. The color scale method was employed for quantitative visualization, differences between size, magnitude, and complexity of vorticity concentrations are seen clearly. The distributions of the instantaneous vorticity patterns, ω are determined using the corresponding instantaneous velocity components, v and w of the flow area of each image before determining the time-averaged vorticity, $<\omega^*>$ patterns using experimental data of the PIV system. The dimensionless time-averaged vorticity concentration is formulated as $<\omega^*>= <\omega>C/U$ where $<\omega>$ is time-averaged vorticity concentration (1/s), U is the free-stream velocity (m/s) and C (m) is the chord length of the delta wing. Minimum and gradually increasing values of patterns of time-averaged vorticity are taken with the same scale at the same angle of attack, α, and the sideslip angle, β over crossflow planes to make a comparison between different experimental cases. The time-averaged patterns of dimensionless vorticity concentrations, $<\omega^*>$ rotating clockwise and counterclockwise do not have exact similarity between

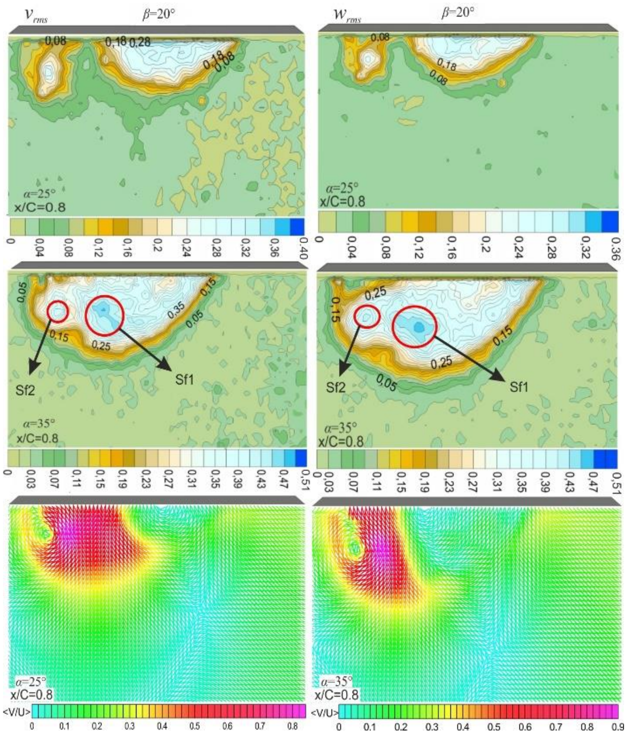

Fig. 7 Distributions of v_{rms}, w_{rms} and $<V/U>$at *x/C*=0.8 for α=25° and α=35°, respectively

them under the influence of β. It is known that vortex bursting is often referred to as the main production source of unstable vortex concentrations with various sizes.

Under any degree of α and β, the size of the flow domain and the magnitude of vorticity concentrations on the leeward and windward sides in crossflow planes differ

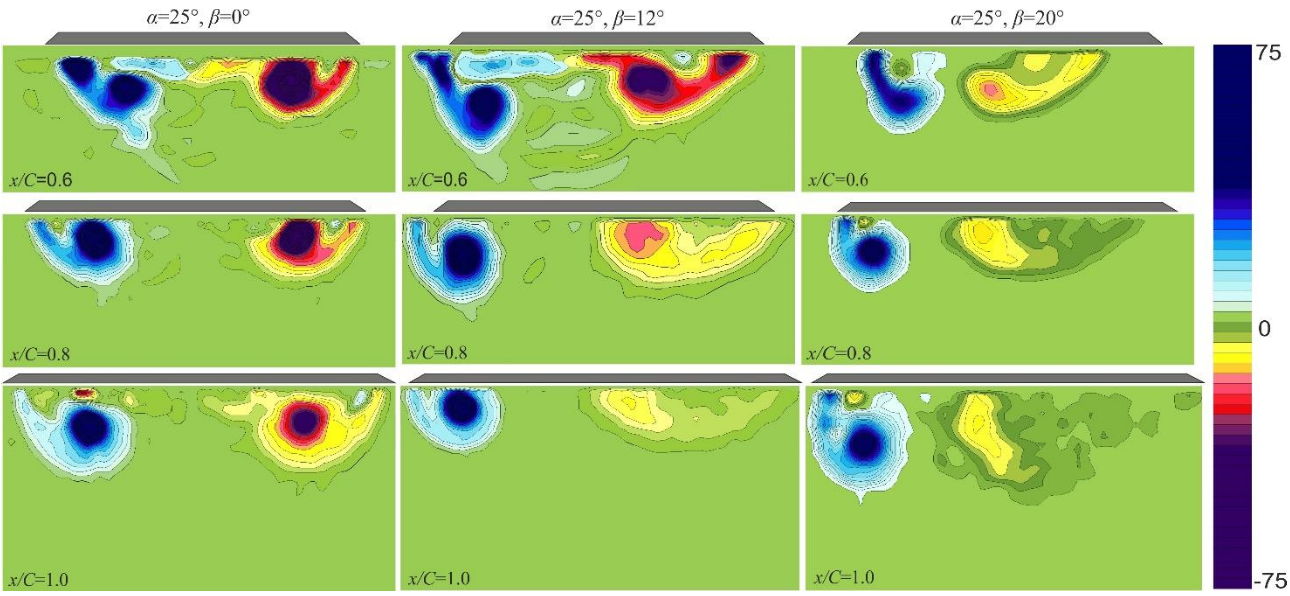

Fig. 8 Patterns of time-averaged dimensionless vorticity, $<\omega^*>$ for sideslip angles ranging from β=0° to 20° and the locations of crossflow planes ranging from x/C=0.6 to 1.0 for α=25°

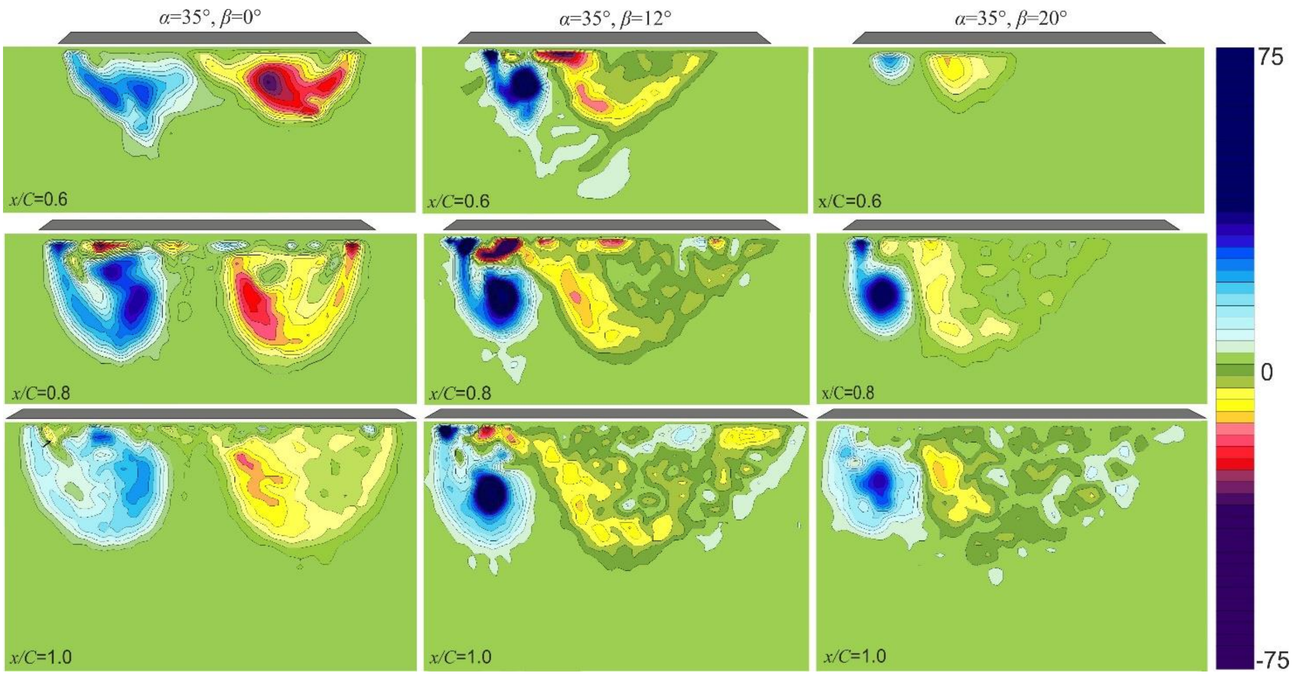

Fig. 9 Patterns of time-averaged dimensionless vorticity, $<\omega^*>$, for sideslip angles ranging from β=0° to 20° and the locations of crossflow planes ranging from x/C=0.6 to 1.0 for α=35°

slightly before the onset of vortex bursting. However, as seen in columns 2-3 in Figs. 8 and 9, these vorticity concentrations, $<\omega^*>$ downstream of the point of the primary vortex bursting have dissimilarities regarding the size of the reversed flow domain and the magnitude as well as for settling places based on the reference line which is the central chord axis of the delta wing. The dissimilarity of vortical flow structures is amplified by the variation of α and β and x/C. For example, as seen in column 1 in Fig. 8 and in line 1 column 1 in Fig. 9, the contours of the dimensionless time-averaged vorticity concentration, $<\omega^*>$ having α=25° and α=35° at x/C=0.6, 0.8 and 1.0 indicates a well-defined vorticity concentration clusters before the onset of vortex bursting. However, there are several small-scale vorticity concentrations which take place after the point of the primary vortex bursting on the windward side, particularly at β=20° and x/C=0.8 and 1.0 as seen in Fig. 9. Setting the delta wing with α=35° and β=20°, the absolute flow separation occurs from a large part of the delta wing surface as seen in Fig. 9.

In this flow separation region, several positive and negative vorticity concentrations occur. The separated flow area occupies most of the delta wing surface as seen in line 3 column 3 in Fig.8 and in line 2-3 columns 2-3 in Fig. 9.

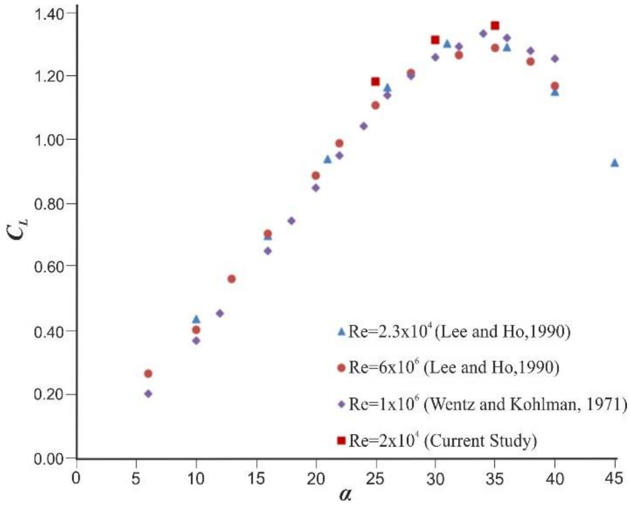

Fig. 10 Variation of lift coefficient, C_L against the ang le of attack, α in case of β=0° and comparisons of the present results with the previous studies from the litera ture

In general, the size and the magnitude of the vorticity concentrations on the leeward side are more significant than the windward side as systematically shown in crossflow planes. The structure of the vortical flow on both sides is influenced by side-slipping delta wing. It is also revealed by most presentations of flow properties that the central point of vorticity concentrations or swirling flows move in the lateral directions towards the leeward side, particularly at x/C=1.0. As a result of observing animations of a quantitative representations of instantaneous vorticity patterns, ω in connection with time-averaged vorticity patterns, $<\omega^*>$ presented in Figs. 8 and 9 revealed that an irregular vorticity concentration can potentially contribute to buffeting the adjacent aerodynamic surface as long as instability of those non-symmetrical vorticity concentrations are exhibited.

As shown in Fig. 10, it is observed that the current results of lift coefficient, C_L with angles of attack, α at β=0° are good agreement with those data from Lee and Ho (1990) and Wentz and Kohlman (1971). It was observed that the effects of parameters such as experimental uncertainties, the thickness/chord ratio and the bevel angle of the delta wing did not have great effects on the results presented in Fig. 10. For instance, as the delta wing tested by Wentz and Kolhman (1971) at Re=1x10^6 has a bevel angle of 15° at leading and trailing edges of the delta wing.

Variations of the lift and drag coefficients, C_L and C_D with the sideslip angle, β for α=25° and 35° are given in Fig. 11. Depending on the increase in sideslip angles, β at α=35°, there is a significant decrease in C_L value. As β is gradually upgraded, the reduction in C_L was 3% when β value is altered from 0° to 4°. However, when β value is brought to 8°, a sudden drop, approximately 15% reduction in C_L is observed comparing to β=0° case. When β value is gradually increased to 20°, the total C_L drop was calculated as 22%. In the case of α=25°, the change of C_L is observed which is more linear according to angle of attack of α=35°. In the case of α=25°, there is a more serious drop in total C_L

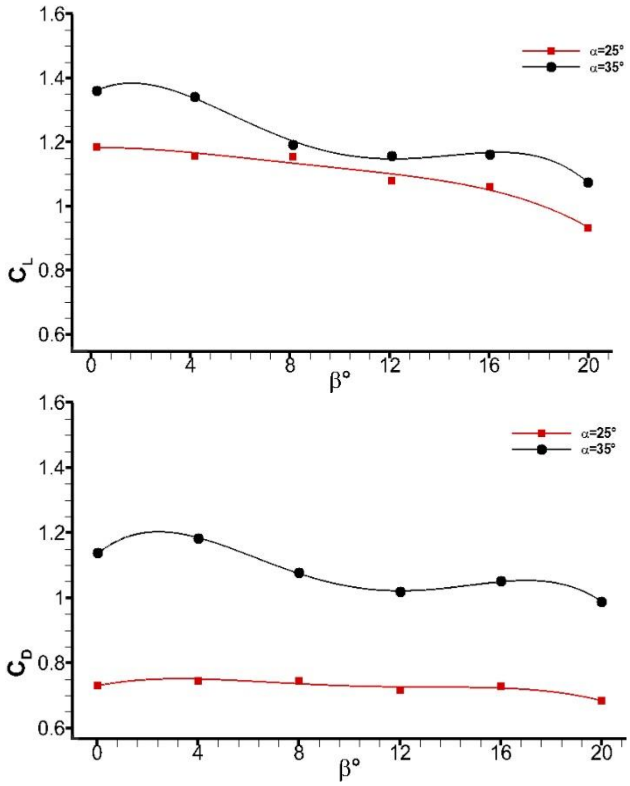

Fig. 11 Variation of lift coefficient, C_L and C_D for α=25° and 35° with the variation of β

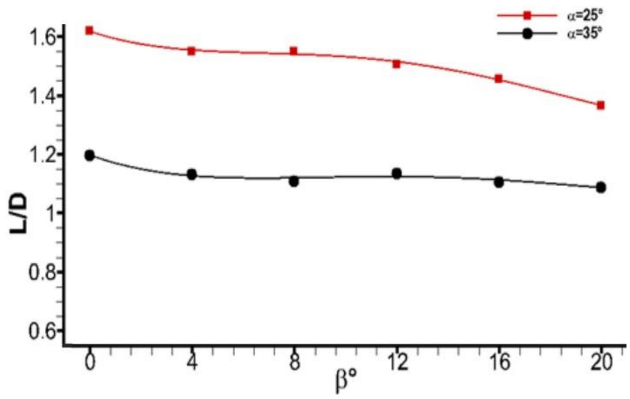

Fig. 12 Variation of the lift/drag coefficient, C_L/C_D ratio for α=25° and 35° with the variation of β

than α=35°. When β value is changed from 0° to 20°, the total percentage of drop in the lift coefficient, C_L is approximately as 27.5%.

A very slight increase in C_D was observed at all angles of attack, α when the value of β was given as 4° and then, C_D values were gradually decreased. The percentage of the decrease in C_D under the variation of β is less than C_L. It has been determined that C_L value is more sensitive to the increase of α under the variation of β. The reduction in C_D at β=20° compared to β=0° is about 6.5% for α=25° and the reduction in C_D is about 13% for α=35°.

As shown in Fig. 12, the ratio of the lift coefficient to the drag lift coefficient, C_L/C_D demonstrates the effect of β on the aerodynamic performance of the delta wing. This ratio generally tends to decrease gradually with increasing β

for both angles of attack of α=25° and α=35°. Throughout the range of 0°≤β≤20° considered the C_L/C_D ratio at α=25° is always higher than the case of α=35°. The value of C_L/C_D is equal to 1.63 for α=25° and β=0°. When β value is increased to 20°, a gradual decrease in the C_L/C_D ratio happens which corresponds to 15.7% reduction at α=25° and 9% reduction occurs in the ratio of C_L/C_D at α=35°.

5. Conclusions

In crossflow planes, time-averaged flow data shows that there is an identical flow characteristic on both sides of a midline of images in the case of β equal to zero. The present experimental results reveal that symmetrical flow composition over measuring planes deteriorates as β is upgraded. On one hand, the leading-edge vortex bursting on the leeward side travels away in the downstream of the flow direction from the rear end of the delta wing. On the other hand, the points of the leading-edge vortex bursting near the windward side move towards the tip of the delta wing. Vorticity concentrations with different magnitudes interact with the delta wing surface causing unsteady buffet loading which increases with the enlargement of β.

The foci, F_1 and F_2 generally encounter the central point of well-defined reverse flow presented by time-averaged streamlines, $<\Psi>$. Both foci and saddle points move away slowly from the delta wing surface in downwards direction and those points approach each other gradually when α is enlarged with the increase of β. Counter-rotating flow circulations defined by patterns of streamlines, $<\Psi>$ that occur on both sides of the chord axis are dissimilar concerning their sizes and magnitudes.

The central zone of maximum values of v_{rms} and w_{rms} moves away from the delta wing surface towards the central points of the swirling flow domain where the magnitudes of the highest time-averaged RMS velocity component measured at α=35°. Swirling flow 1, Sf_1 which takes place on the windward side expands large enough to interact significantly with Swirling flow 2, Sf_2.

Vorticity concentrations, $<\omega^*>$ downstream of the primary vortex bursting have dissimilarities regarding the size of the reversed flow domain. The magnitude and this dissimilarity of vortical flow structures are amplified by the variation of α, β, and x/C. The central point of vorticity concentrations or swirling flows moves in the lateral directions towards the leeward side, particularly, at x/C=1.0.

The test results show that the lift coefficient, C_L is reduced by 27.5% for α=35° and β=20°, on the other hand, C_L is reduced by 22% for α=25° and β=20°. The reduction in the drag coefficient, C_D is about 13% for β=20° and α=35°. Also, the reduction in the drag coefficient, C_D is about 6.5%, for β=20° and α=35°. Finally, the increase of α and β causes a considerable reduction in the lift force, F_L, more than in the drag force, F_D. The results obtained from quantitative and qualitative experiments reveal that the aerodynamic structures cause non-uniform F_L and F_D and non-homogeneous buffet loading over the delta wing surface under the variations of β which may cause an unbalanced rolling moment.

Acknowledgments

The research described in this paper was financially supported by the Scientific and Technological Research Council (TUBITAK) of Turkey under contract no: 114M497. Additional financial support was also received from the Scientific Research Project Office of Çukurova University under contract no: FYL-2016-5845.

References

Canpolat, C., Yayla, S., Sahin, B. and Akilli, H. (2009), “Dye visualization of the flow structure over a yawed nonslender delta wing”, *J. Aircraft*, **46**, 1818-1822. https://doi.org/10.2514/1.45274.

Canpolat, C., Yayla, S., Sahin, B. and Akilli, H. (2012), “Observation of the vortical flow over a yawed delta wing”, *J. Aerosp. Eng.*, **25**(4), 613-626. https://doi.org/10.1061/(ASCE)AS.1943-5525.0000163.

Chen, M., Liu, P., Guo, H. and Qu, Q. (2015), “Effect of sideslip on high-angle-of-attack vortex flow over close-coupled canard configuration”, *J. Aircraft*, **53**, 217-230. https://doi.org/10.2514/1.C033305.

Delery, J.M. (1994), “Aspects of vortex breakdown”, *Progress Aerosp. Sci.*, **30**, 1-59. https://doi.org/10.1016/0376-0421(94)90002-7.

Erickson, G., Schreiner, J. and Rogers, L. (1989), “On the structure, interaction, and breakdown characteristics of slender wing vortices at subsonic, transonic, and supersonic speeds”, *In 16th Atmospheric Flight Mechanics Conference.*

Ericsson, L.E. (1992), “Sources of high alpha vortex asymmetry at zero sideslip”, J. Aircraft, **29**(6), 1086-1090.

Escudier, M. (1988), “Vortex breakdown: Observations and explanations”, *Progress Aerosp. Sci.*, **25**, 189-229. https://doi.org/10.1016/0376-0421(88)90007-3.

Gursul, I. and Wang, Z. (2018), “Flow control of tip/edge vortices”, *AIAA J.*, **56**(5), 1731-1749. https://doi.org/10.2514/1.J056586.

Gursul, I., Gordnier, R. and Visbal, M. (2005), “Unsteady aerodynamics of nonslender delta wings”, *Progress Aerosp. Sci*., **41**, 515-557.

Hall, M.G. (1972), “Vortex breakdown”, *Annu. Rev. Fluid Mech.*, **4**(1), 195-218. https://doi.org/10.1146/annurev.fl.04.010172.001211.

Johnson, Jr., Joseph, L., Grafton, S.B. and Long, P. (1980), “Exploratory investigation of the effects of vortex bursting on the high angle-of-attack lateral-directional stability characteristics of highly-swept wings.”, A Collection of Technical Papers, *AIAA 11th Aerodynamic Testing Conference*, Colorada, March.

Karasu, I., Sahin, B., Akilli, H. and Canpolat, C. (2015), “Dye visualization of a yawed slender delta wing”, *J. Therm. Eng.*, **1**(2), 646-654.

Ke, S.T., Zhu, P. and Ge, Y.J. (2019), “Effects of different wind deflectors on wind loads for extra-large cooling towers”, *Wind Struct.*, **28**(5), 299-313. https://doi.org/10.12989/was.2019.28.5.299.

Lee, M. and Ho, C.M. (1990), “Lift force of delta wings”, *Appl. Mech. Rev.*, **43**(9), 209-221. https://doi.org/10.1115/1.3119169.

Lu, Z.Y. and Zhu, L.G. (2004), “Study on forms of vortex breakdown over Delta Wing”, *Chinese J. Aeronaut.*, **17**, 13-16. https://doi.org/10.1016/S1000-9361(11)60196-9.

Lucca-Negro, O. and O’Doherty (2001), “Vortex bursting: A review”, *Progress Energy Combustion Sci.*, **27**(4), 431-481.

Meng, X., Liu, F. and Luo, S. (2018), “Effect of low dorsal fin on the breakdown of vortices over a slender delta wing”, *Aerosp.*

Sci. Technol., **81**, 316-321. https://doi.org/10.1016/j.ast.2018.08.017.

Menke, M., Yang, H. and Gursul, I. (1996), “Further experiments on fluctuations of vortex breakdown location”, *The 34th Aerospace Sciences Meeting and Exhibit*. https://doi.org/10.2514/6.1996-205.

Nelson, R.C. and Pelletier, A. (2003), “The unsteady aerodynamics of slender wings and aircraft undergoing large amplitude maneuvers”, *Progress Aerosp. Sci.*, **39**(2-3), 185-248. https://doi.org/10.1016/S0376-0421(02)00088-X.

Ozgoren, M., Sahin, B. and Rockwell, D. (2002), “Vortex structure on a Delta Wing at high angle of attack”, *AIAA J.*, **40**, 285-292. https://doi.org/10.2514/2.1644.

Ozturk, N.A., Akkoca, A. and Sahin, B. (2008), “PIV measurements of flow past a confined cylinder”, *Experiments Fluids*, **44**(6), 1001-1014. https://doi.org/10.1007/s00348-007-0459-z.

Payne, F.M. and Nelson, R.C. (1986), “Experimental investigation of vortex bursting on a Delta Wing”, *NASA Technical Report*, Report No. N86-27196.

Sahin, B., Akilli, H., Lin, J.C. and Rockwell, D. (2001), “Vortex breakdown-edge interaction: consequence of edge oscillations”, *AIAA J*., 39, 865-876. https://doi.org/10.2514/2.1390.

Sahin, B., Yayla, S., Canpolat, C. and Akilli, H. (2012), “Flow structure over the yawed nonslender diamond wing”, *Aerosp Sci Technol*, **23**, 108-119. https://doi.org/10.1016/j.ast.2011.06.008.

Shields, M. and Mohseni, K. (2012), “Effects of sideslip on the aerodynamics of low-aspect-ratio low-Reynolds-number wings”, *AIAA J.*, **50**(1), 85-99. https://doi.org/10.2514/1.J051151.

Soloff, S.M. and Meinhart, C.D. (1999), CLEANVEC: PIV Vector Validation Software. Available from the Laboratory for Turbulence and Complex Flow at the University of Illinois, U.S.A.

Sun, H. and Ye, J. (2016), “3-D characteristics of conical vortex around large-span flat roof by PIV technique”, *Wind Struct.*, **22**(6), 663-684. https://doi.org/10.12989/was.2016.22.6.663.

Taylor, G.S. and Gursul, I. (2004), “Buffeting flows over a low-sweep delta wing”, *AIAA J.*, **42**(9), 1737-1745. https://doi.org/10.2514/1.5391.

Verhagen, N. (2000), “Effect of Sideslip on the Flow over a 65-deg Delta Wing”, *In the 38th Aerospace Sciences Meeting and Exhibit*.

Verhagen, N.G. and Jobe, C.E. (2003), “Wind-tunnel study on a 65-deg Delta Wing at sideslip”, *J. Aircraft*, **40**, 290-296. https://doi.org/10.2514/2.3092.

Wentz, Jr., W.H. and Kohlman, D.L. (1971), “Vortex breakdown on slender sharp-edged wings”, *J. Aircraft*, **8**(3), 156-161. https://doi.org/10.2514/3.44247.

Williamson, C.H.K. and Govardhan, R. (2004), “Vortex-induced vibrations”, *Annu. Rev. Fluid Mech.*, **36**, 413-455. https://doi.org/10.1146/annurev.fluid.36.050802.122128.

Yaniktepe, B. and Rockwell, D. (2004), “Flow structure on a Delta Wing of low sweep angle”, *AIAA J.*, **42**(3), 513-523. https://doi.org/10.2514/1.1207.

Yaniktepe, B. and Rockwell, D. (2005), “Flow structure on diamond and lambda planforms: trailing-edge region”, *AIAA J.*, **43**(7), 1490-1500. https://doi.org/10.2514/1.7618.

Yayla, S., Canpolat, Ç. Sahin, B. and Akilli, H. (2010), “Yaw angle effect on flow structure over the nonslender diamond wing”, *AIAA J.*, **48**(10), 2457-2461. https://doi.org/10.2514/1.J050380.

Yayla, S., Canpolat, C., Sahin, B. and Akilli, H. (2013), “The effect of angle of attack on the flow structure over the nonslender lambda wing”, *Aerosp. Sci. Technol.*, **28**(1), 417-430. https://doi.org/10.1016/j.ast.2012.12.007.

Ye, J. and Dong, X. (2014), “Improvement and validation of a flow model for conical vortices”, *Wind Struct.*, **19**(2), 113-144. https://doi.org/10.12989/was.2014.19.2.113.

Zharfa, M., Ozturk, I. and Yavuz, M.M. (2016), “Flow structure on Nonslender delta wing: Reynolds number dependence and flow control”, *AIAA J.*, Vol. **54**(3), 880-897. https://doi.org/10.2514/1.J054495.

CC